Received 27 October 2020; revised 26 December 2020; accepted 4 January 2021. Date of publication 11 January 2021; date of current version 25 February 2021. The review of this article was arranged by Editor S. Ikeda.

Digital Object Identifier 10.1109/JEDS.2021.3050801

Sheet Resistance Reduction of MoS_2 Film Using Sputtering and Chlorine Plasma Treatment Followed by Sulfur Vapor Annealing

TAKUYA HAMADA [1], SHIGETAKA TOMIYA [2], TETSUYA TATSUMI [2], MASAYA HAMADA [1], TAIGA HORIGUCHI [1], KUNIYUKI KAKUSHIMA [3] (Member, IEEE), KAZUO TSUTSUI [4] (Senior, Member, IEEE), AND HITOSHI WAKABAYASHI [1] (Senior, Member, IEEE)

1 Department of Electrical and Electronic Engineering, School of Engineering, Tokyo Institute of Technology (Suzukakedai Campus), Yokohama 226-8503, Japan
2 Research Institute for the Earth Inclusive Sensing, Tokyo Institute of Technology (Suzukakedai Campus), Yokohama 226-8503, Japan
3 Tokyo Institute of Technology, Yokohama 226-8503, Japan
4 Interdisciplinary Graduate School of Science and Engineering, Tokyo Institute of Technology, Yokohama 152-8550, Japan

CORRESPONDING AUTHOR: T. HAMADA (e-mail: hamada.m..af@m.titech.ac.jp)

This work was supported in part by the Collaborative Research Program founded by Sony Corporation and in part by the Japan Science and Technology Agency Center of Innovation Program (JST COI) under Grant JPMJCE1309.

ABSTRACT Sheet resistance (R_{sheet}) reduction of a-few-layered molybdenum disulfide (MoS_2) film using sputtering is investigated in this study. To enhance the carrier density, chlorine (Cl_2) gas excited by inductively coupled plasma is introduced as a substitute for sulfur. To electrically activate the Cl dopants and simultaneously prevent out-diffusion of sulfur, a furnace annealing was performed in sulfur-vapor ambient. Consequently, the R_{sheet} in the MoS_2 film with the Cl_2 plasma treatment remarkably reduced by one order lower than that without one, because of the activation of Cl dopants in the MoS_2 film.

INDEX TERMS Activation annealing, chlorine plasma, molybdenum disulfide (MoS_2), radio-frequency magnetron sputtering, transition metal dichalcogenide (TMDC).

I. INTRODUCTION

MoS_2 film which is one of the transiton metal dichalcogenides (TMDCs) has attracted great attentions, because of its excellent electrical and physical properties such as its high mobility even at atomically thin thickness, adequate band-gap, flexibility and transparency [1]–[4] for advanced LSIs, energy harvesters, displays and sensors [5]–[10]. To obtain an atomically thin MoS_2 film with large area for such applications, a chemical vapor deposition (CVD) method is considered. However, to synthesize large MoS_2 film on substrate, a special treatment with alkali metal is used [11], [12], that influences in the Fermi-level pinning near the conduction band minimum [13]. As a method to avoid the unexpected difficulties and achieve large films, a sputtering method under ultra high vacuum (UHV) has been proposed as a physical vapor deposition (PVD) [14], [15]. For the Seebeck device in thermoelectric generator as an energy harvester, high efficiency of energy conversion was achieved in a sputtered MoS_2 film by low thermal conductivity [16]. However, sulfur atoms are easily out-diffused from the MoS_2 film during sputtering process, which cause high carrier density. We have found that sulfur vapor annealing (SVA) compensates for S defects resulting in a carrier density reduction down to 1.8 $\times$ 10^{16} cm^{-3} and also a mobility enhancement [17], [18]. Furthermore, normally-off nMISFETs with an appropriate threshold voltage were performed, because of the low carrier density in MoS_2 film formed by sputtering and treated by SVA and an appropriate work function of metal gate [19].

To intentionally enhance the carrier density in low carrier-density MoS_2 film for the Seebeck device, intrinsic and extrinsic carrier generations are expected. Although the intrinsic technique such as vacancies and interstitials of the consisting materials generates several energy levels in the band gap [20]–[22], the extrinsic technique is favorable rather than intrinsic one to significantly enhance the carrier density with high controllability [23], for which electrostatic doping [24], molecular adsorption [25]–[27] and substitutional doping [28]–[33] can be considered. Although electrostatic

This work is licensed under a Creative Commons Attribution 4.0 License. For more information, see https://creativecommons.org/licenses/by/4.0/

doping has high carrier density, a device structure is complex. And molecular adsorption is unstable on thermodynamics. Therefore, substitutional doping technology is selected in this study, because of its simple structure and stability. Since high carrier mobility is required to enhance the power factor (PF) of the Seebeck device, an n-type MoS_2 film is selected rather than p-type one [34], [35]. As candidates for the n-type dopant, Group 7 and 17 elements were examined as substitution for molybdenum (Mo) and S, respectively. In terms of ionization and formation energies, chlorine (Cl) substituting for S was selected as the n-type dopant in the MoS_2 film [36], [37]. For the fabrication method, ion implantation and plasma exposure in dopant ambient have been investigated [28]–[31]. However, energetic dopants in these methods can generate S vacancies and an activation of dopants in the MoS_2 film is required [31].

In this study, we investigates the combination of Cl_2-plasma treatment and SVA for sheet resistance reduction in MoS_2 films formed by sputtering.

II. EXPERIMENTAL METHODS

To examine the sheet resistance in the MoS_2 film, a circular transmission line model (CTLM) pattern was used, as shown in Fig. 1 [38]–[40]. A base material of silicon dioxide (SiO_2) on a silicon substrate was cleaned in a wet process using a piranha solution. Titanium-nitride (TiN) electrodes of 40 nm thickness were formed by sputtering and wet etching with H_2O_2. The MoS_2 films were formed using an ultra-high vacuum (UHV) radio frequency (RF) magnetron sputtering tool with MoS_2 target of 99.99% purity, at a substrate temperature of 300°C, under argon (Ar) pressure of 0.55 Pa, an Ar flow rate of 7 sccm, an RF power of 40 W and a distance of 150 mm between the MoS_2 target and the substrate. We note that the sputter-deposited MoS_2 film has layered structure in parallel to the substrate because of high temperature at 300°C. The detail of the film was investigated in our previous work [18]. The MoS_2 films were exposed to a Cl_2 plasma generated using an inductive coupling plasma reactive ion etching (ICP-RIE) tool (SAMCO RIE-101iPH), under Cl_2) pressures from 0.4 to 3.2 Pa, with a Cl_2 flow rate of 7 sccm, ICP powers from 5 to 20 W, for 20 to 160 s. Herein, the bias power is set to 0 W resulting in a floating potential at the sample. The MoS_2 films were annealed by SVA at the 700°C in a sulfur ambient under 100 Pa for 40 min to activate the dopants and compensate for the sulfur vacancies, simultaneously. The thickness of the MoS_2 film was approximately 2.0 nm measured using the X-ray reflection (XRR) method. Sheet resistances in the MoS_2 film were extracted from the CTLM measurement with spacing from 5 to 30 μm and r = 90 μm.

Raman spectroscopy was performed at 532 nm wavelength and pseudo-Voigt function was used to fit the Raman spectrum of the MoS_2 film. An atomic force microscope (AFM) was performed in dynamic force microscope (DFM) mode. The changes in the thickness of the MoS_2 layer with and without the Cl_2 plasma treatment were observed using transmission electron microscopy (TEM) with an accelerating voltage of 200 keV. An X-ray photoelectron spectroscopy (XPS) using an Al K_α X-ray source was also performed with spectral fitting using the pseudo-Voigt function. The composition ratio of the MoS_2 film is expressed as follows:

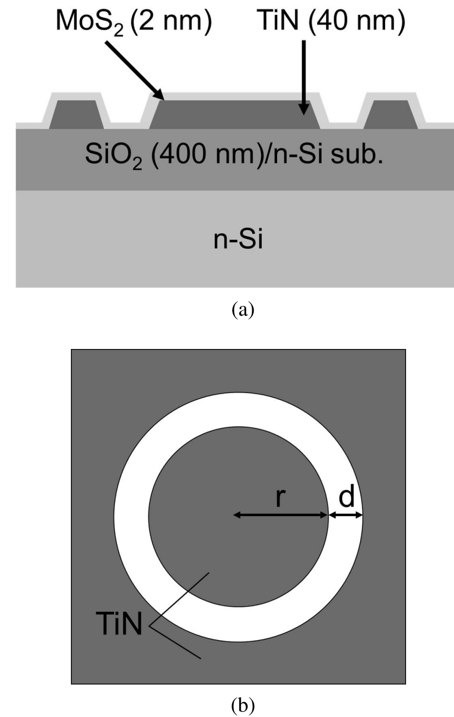

FIGURE 1. Schematic illustrations of the CTLM pattern with TiN contacts and MoS_2 film. (a) Cross-sectional and (b) top views with r = 90 μm and several contact distances d from 5 to 30 μm.

$$C_i = \frac{A_i/\mathrm{RSF}_i}{\sum_j A_j \mathrm{RSF}_j} \tag{1}$$

where C_i, A_i, and RSF_i are the composition ratio, peak area, and relative sensitivity factor of the atom i, respectively [17]. Depth profiling of time-of-flight secondary ion mass spectroscopy (TOF-SIMS) were performed using bismuth and cesium ions as the primary and sputtering ion sources, respectively.

III. RESULTS AND DISCUSSION

To evaluate the sheet resistance reduction in the MoS_2 film, typical results from CTLM with and without Cl_2 plasma treatment are shown in Fig. 2, as a function of the contact distance at 5 W under 0.4 Pa for 40 s. The total resistance depending on contact distance is shown in following Equation (2),

$$R_{total} = \frac{R_{sheet}}{2\pi}\left[\frac{L_t}{r} + \frac{L_t}{r+d} + \ln\left(1+\frac{d}{r}\right)\right] \tag{2}$$

where R_{sheet}, L_t, r, and d are the sheet resistance, transfer length, inner radius, and contact distance, respectively. The R_{sheet} of 8.50 MΩ/sq. with the Cl_2 plasma treatment is

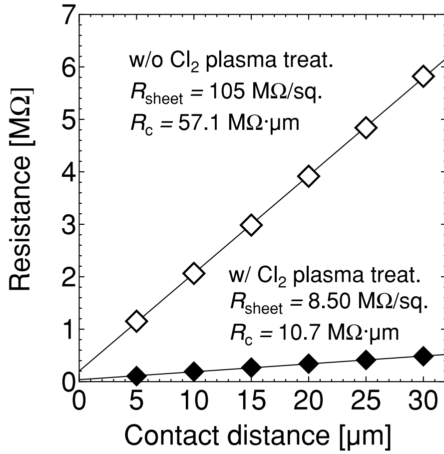

FIGURE 2. Resistance dependence on contact distance in MoS_2 films with and without Cl_2 plasma treatment at 5 W under 0.4 Pa for 40 s, followed by the SVA.

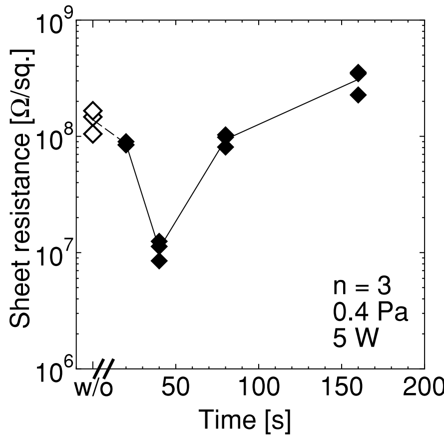

FIGURE 3. Sheet resistance of MoS_2 film as a function of Cl_2 plasma exposure time. The duration time was varied at 5 W under 0.4 Pa. SVA was applied at 700°C for 40 min.

approximately ten times less than that of 105 MΩ/sq. without the treatment. Furthermore, the contact resistance normalized by the channel width decreases down to 1.07 kΩ.cm. Both sheet and contact resistances are significantly reduced by the Cl_2 plasma treatment.

In order to further reduce the resistance of the MoS_2 film, a sheet resistance dependence on plasma exposure time is shown in Fig. 3. R_{sheet} decreases and increases with an increase in plasma exposure time up to and beyond 40 s, respectively. It is speculated that the resistance reduction is because of an increase in the quantity of Cl dopants.

To discuss the cause of increase in the resistance, cross-sectional TEM images were examined, as shown in Figs. 4(a), (b), and (c) for each exposure time of the Cl_2 plasma treatment. The thickness with Cl_2 plasma treatment for 40 s approximately equals to that without treatment. However, the thickness of the MoS_2 film with exposure time of 160 s is thinner than that of 40 s maintaining the layered structure and the uniformity of the film thickness, as shown in Fig. 4(c). This is because due to etching influences.

To explain the sheet resistance characteristics consisting of both doping and etching at the same time, we assume the following conditions. Initially, the conductance (G_n) of the n-th layer from the top layer of the MoS_2 film as a function of the exposure time t of the Cl_2 plasma is expressed as

$$G_n(t) = \frac{1}{R_n(t)} = A^{n-1}B(t - t_{incubation}) + G_{initial}, \quad (3)$$

where A, B, $t_{incubation}$, and $G_{initial}$ are ratio of conductance increase on the number of layer, conductance increase over time, incubation time to stabilize the Cl_2 plasma and an incremental conductance at 0 s, respectively. If t was less than $t_{incubation}$, $G_n(t)$ is equal to $G_{initial}$. Therefore, the sheet resistance $R_{sheet}(t)$ is given by

$$R_{sheet}(t) = \frac{1}{\sum_n G_n(t)}. \quad (4)$$

Furthermore, we assume that the top layer of the MoS_2 film is etched in the order with top-S, middle-Mo and bottom-S by the Cl_2 plasma with a low ICP power [41], as shown in Fig. 4(c). Moreover, if the middle-Mo remained after etching, the S-Mo-S structure in the layer is going to be recovered by the SVA [17]. Under these speculations, if the middle-Mo in the top layer was not etched, the sheet resistance decreases with an increase in exposure time, because of the doping effect of less than 40 s, as shown in Fig. 3. In contrast, if the middle-Mo was etched, it is difficult to reduce the sheet resistance any more. Therefore these phenomena are expected in a cyclic manner, which is consistent with experimental results, as shown with dotted lines in Fig. 5 Eventually, the minimum R_{sheet} at an exposure time of 40 s is approximately ten times less than that without treatment.

To confirm improvements in crystallinity of low resistance MoS_2 film, the Raman spectra with and without plasma treatment are shown in Fig. 6. The peaks of E^1_{2g} (in-plane vibration mode of Mo and S) and A_{1g} (out-of-plane mode vibration of S) were observed even after Cl_2 plasma treatment. Fig. 7 shows the full width at half maximum (FWHM) values of E^1_{2g} and A_{1g} with and without the Cl_2 plasma treatment followed by the SVA. The FWHM values increase after the plasma treatment. this is due to the damaged crystallinity of MoS_2 film by the Cl_2 plasma treatment. On the other hand, although the FWHM values of the film significantly decrease after the SVA, the FWHM values with the Cl_2 plasma treatment are still greater than those without treatment, because of disorder of phonon can be considered due to Cl dopants.

Root mean square (RMS) values of the roughness obtained by the AFM, as shown in Fig. 8, increase after the plasma treatment and decrease by the SVA, whose trend is consistent with the changes in crystallinity discussed on the Raman spectra in Fig. 7.

To discuss the dopant characteristics, a resistivity depending on temperature is modeled using the thermally activated

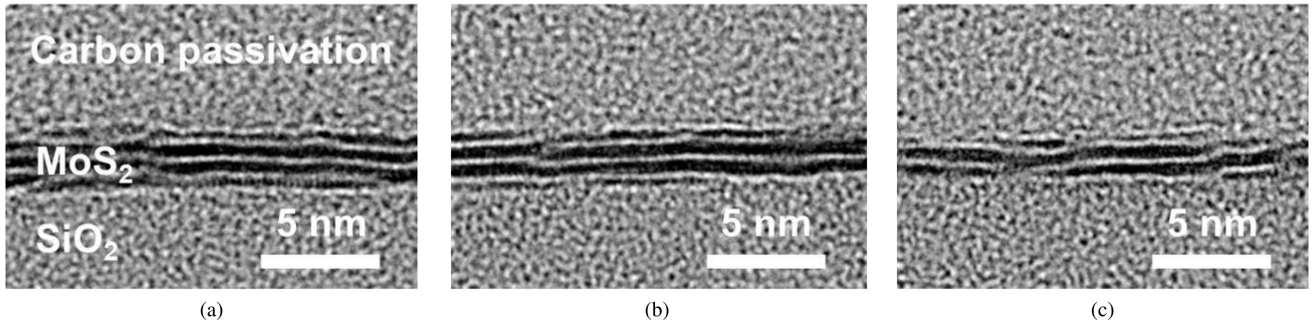

FIGURE 4. Cross-sectional TEM images of MoS_2 film depending on Cl_2 plasma exposure times of (a) no exposure, (b) 40 s, and (c) 160 s, each followed by SVA.

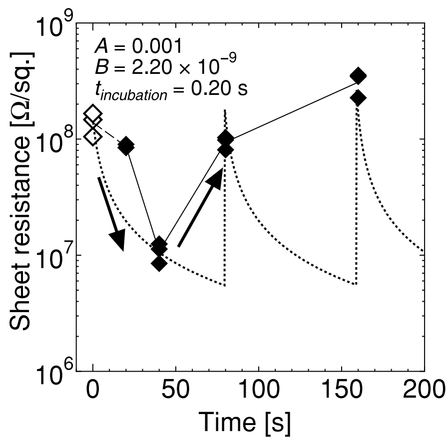

FIGURE 5. Comparison of the model and experimental results on sheet resistance of the MoS_2 film as a function of the Cl_2 plasma exposure time. The dotted line shows the calculated sheet resistance in the MoS_2 film from the model, and the value at 0 s corresponds to that without the Cl_2 plasma treatment.

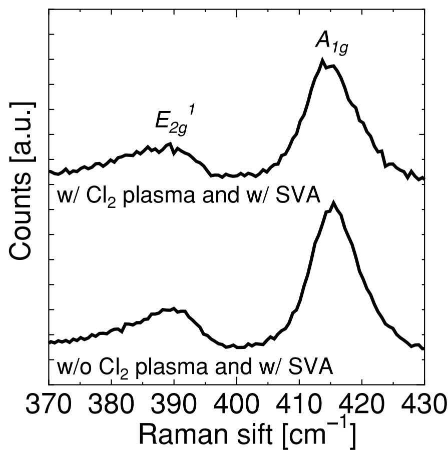

FIGURE 6. Raman spectra of MoS_2 films with and without Cl_2 plasma treatment at 5 W under 0.4 Pa for 40 s followed by SVA.

transport equation [42]:

$$\rho = \frac{1}{\sigma} = \frac{1}{qn(T)\mu(T)} = \frac{1}{\sigma_0(T)} \exp\left(\frac{E_a}{k_B T}\right) \tag{5}$$

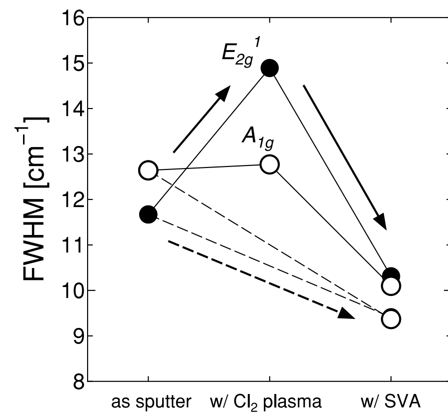

FIGURE 7. FWHM values in E^1_{2g} and A^1_g of the Raman spectra for MoS_2 films along each process. The dotted lines connect the FWHM values without the Cl_2 plasma treatment.

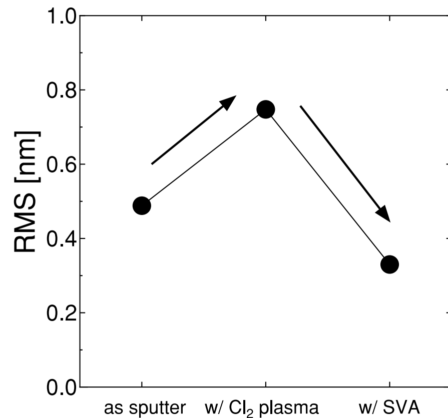

FIGURE 8. RMS values in the AFM of MoS_2 film along process.

where E_a, k_B, and σ_0 are the activation energy, the Boltzmann constant, and pre-factor depending on the temperature, respectively. It has been reported that σ_0 is insensitive at the temperature above 170 K [43], [44]. Therefore, the Arrhenius plot of resistivity in the MoS_2 film was determined using Van der Pauw measurement with 1 cm × 1 cm $MoS_2/SiO_2/Si$ samples patterned with TiN bottom contacts, as shown in Fig. 9. The resistivity values of the MoS_2 film below 170 K

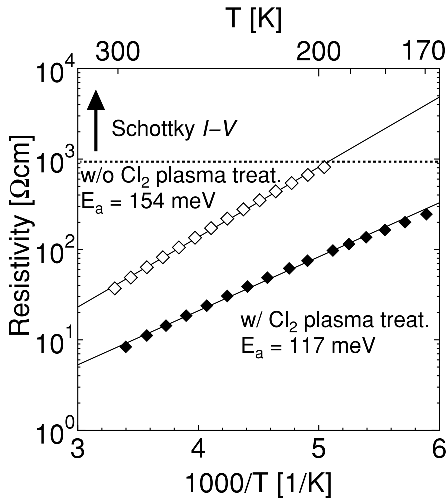

FIGURE 9. Arrhenius plots of resistivity in MoS_2 film with and without Cl_2 plasma treatment at 5 W under 0.4 Pa for 40 s, followed by SVA.

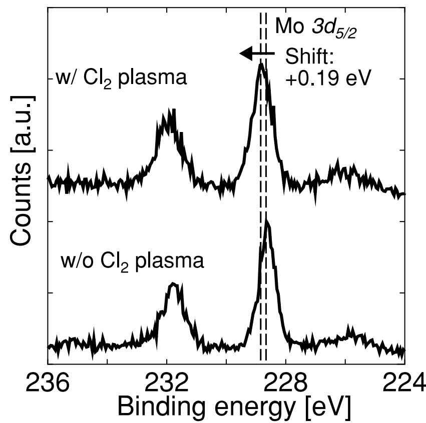

(a)

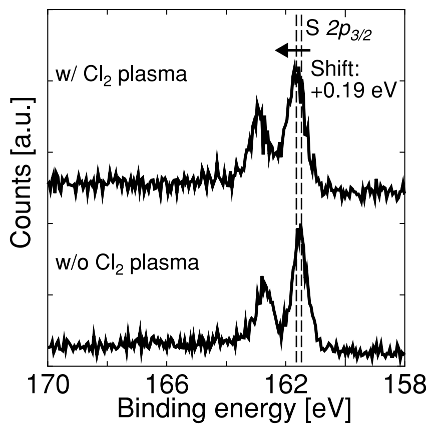

(b)

FIGURE 10. XPS spectra of (a) Mo 3*d* and (b) S 2*p* in the MoS_2 film with and without Cl_2 plasma treatment at 5 W under 0.4 Pa for 40 s, followed by SVA.

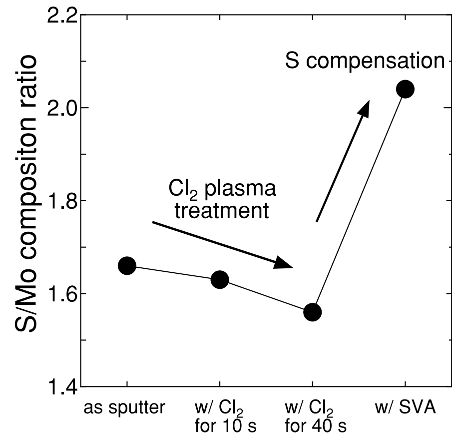

FIGURE 11. S/Mo composition ratio of the MoS_2 film determined from the Mo-S and S-Mo peak areas in the XPS spectra along each process.

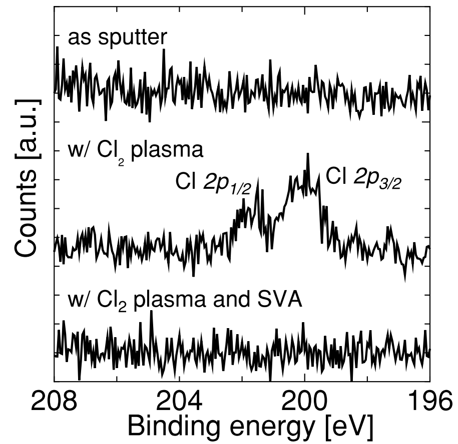

FIGURE 12. XPS spectra of Cl 2*p* in the MoS_2 films along each process.

and 190 K with and without the Cl_2 plasma treatment, respectively, were ignored due to the Schottky $I-V$ characteristics. The activation energies with and without the Cl_2 plasma treatment were 117 and 154 meV, respectively. To validate the polarity of the dopants, XPS analyses of the MoS_2 film surface with and without the Cl_2 plasma treatment were performed. From Figs. 10(a) and (b), the binding energy peaks of Mo $3d_{5/2}$ and S $2p_{3/2}$ shift toward the positive direction. These explain that positive-increases in a position of binding energy peaks correspond to the Fermi level shift approaching to the conduction band minimum.

To discuss the cause of the Fermi level shift to the conduction band minimum, there are two main candidates of S vacancy and Cl doping. A S/Mo composition ratio in the MoS_2 film with the Cl_2 plasma treatment calculated from the Mo-S and S-Mo peak areas in the XPS, presented in Fig. 11, was approximately two. This means that the density of S vacancies in the film was significantly reduced by the SVA. In addition, the ratio slightly decreases with an increase in the duration time of the Cl_2 plasma treatment and a S/Mo ratio of 1.56 with the plasma treatment for 40 s. If the ratio in each layer of 4-layer sputter-deposited MoS_2 film had the same value of 1.66 however only the top-S in the top layer of the film was removed by the plasma, the ratio would be

TABLE 1. Comparisons of electric characteristics in MoS_2 film with various dopants and contact metals, whose mobility and carrier density are simultaneously obtained by the hall effect measurement.

Formation	Thickness [nm]	Contact	Dopant	Type	Hall effect mobility [$cm^2V^{-1}s^{-1}$]	Carrier density [cm^{-3}]	R_{sheet} [Ω/sq.]	Calculated ρ [Ωcm]	R_c [kΩ/μm]	Ref.
Sputtering	2.4	TiN	Cl	n	-	-	8.50×10^6	6.0	1.07×10^4	This work
CVD	13	Ni /Au/Ni	Nb	p	8.5	3.1×10^{20}	1.8×10^3	2.4×10^{-3}	0.6	[45]
CVD	61	Au/Ti	Nb	p	14	3.0×10^{19}	2.5×10^3	1.5×10^{-2}	-	[46]
CVD	1.9×10^5	Au/Ti	Nb	p	7.5	4.3×10^{19}		1.9×10^{-2}	4.98	[47]
CVD	5	Ag	P	p	0.53	1.0×10^{19}	-	1.2	-	[48]
Exfoliation	-	-	Benzyl viologen	n	2.39	2.97×10^{14}	1.0×10^6	4.4×10^2	-	[49]

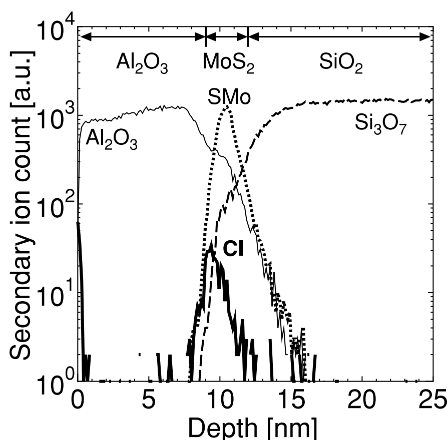

FIGURE 13. TOF-SIMS depth profiles from MoS_2 film in special structure, consisting of Al_2O_3 film on $MoS_2/SiO_2/Si$ with Cl_2 plasma treatment at 5 W under 0.4 Pa for 40 s, followed by the SVA.

reduced down to 1.45. Therefore the etching effect discussed on the sheet resistance reduction is supposed. Fig. 12 shows the Cl 2*p* peaks of Cl_2 plasma treated MoS_2 films together with each process procedure. Although the Cl peaks were detected after the Cl_2 plasma treatment, it is difficult to find them after the Cl_2 plasma treatment and the SVA, due to the detection limit of the XPS evaluation method. Therefore, the TOF-SIMS was performed to determine the existence of chlorine in the MoS_2 film with Cl_2 plasma treatment after SVA, for which an Al_2O_3 film was deposited on the MoS_2 film after the SVA. From the depth profiles in Fig. 13, a Cl ion peak is clearly observed in the MoS_2 film located near the surface without any adsorption on the surface. Moreover, considering with the electrical properties, Cl atoms in the MoS_2 film are successfully activated as n-type dopant during the SVA.

As a benchmark, Table 1 shows comparison of electric characteristics between our result and MoS_2 films applied various doping techniques. Resistivities were calculated from a carrier density and the Hall mobility. Low resistivities in p-type are attributed to degenerative doping over 10^{19} cm^3. In contrast, non-degenerative doping is considered for our technique because the sheet resistance in the doped film is ten times smaller than that with only the SVA, whose carrier density is considered as around 10^{16} cm^3 [17]. On the other hand, low contact resistances for p-type film have been also reported. Although the obtained contact resistance in our n-type work is higher than those due to a wide Schottly barrier width by the relatively low carrier density, the doping technology using combination of Cl_2 plasma and SVA in this article can enable us a good controllability in order of 10^{17} to 10^{18} cm^{-3} of carrier density.

IV. CONCLUSION

Sheet resistance reduction in the MoS_2 film by a combination of Cl_2 plasma and SVA was investigated in the atomic thin film region. The sheet resistance of 8.50 MΩ/sq. with Cl_2 plasma treatment, which is approximately ten times smaller than that without treatment, was observed. The MoS_2 film was successfully doped in n-type with Cl dopants. This technique is promising to control the carrier density in the MoS_2 film for various applications, such as MISFETs and thermoelectric devices.

ACKNOWLEDGMENT

The authors would like to thank Dr. Takuya Hoshii for the variable discussions and his warm supports. Their measurements were supported by Associate Professor Ken Motokura and Open Facility Center at the Tokyo Institute of Technology.

REFERENCES

[1] B. Radisavljevic, A. Radenovic, J. Brivio, V. Giacometti, and A. Kis, “Single-layer MoS_2 transistor,” *Nat. Nanotechnol.*, vol. 6, no. 3, pp. 147–150, Jan. 2011, doi: 10.1038/nnano.2010.279.

[2] S. Das, H.-Y. Chen, A. V. Penumatcha, and J. Appenzeller, “High performance multilayer MoS_2 transistors with scandium contacts,” *Nano Lett.*, vol. 13. no. 1, pp. 100–105, Dec. 2012, doi: 10.1021/nl303583v.

[3] A. Splendiani *et al.*, “Emerging photoluminescence in monolayer MoS_2,” *Nano Lett.*, vol. 10, no. 4, pp. 1271–1275, Mar. 2010, doi: 10.1021/nl903868w.

[4] K. F. Mak, C. Lee, J. Hone, J. Shan, and T. F. Heinz, “Atomically thin MoS_2: A new direct-gap semiconductor,” *Phys. Rev. Lett.*, vol. 105, no. 13, pp. 2–5, Apr. 2010, doi: 10.1103/PhysRevLett.105.136805.

[5] W. P. Risk, G. S. Kino, and H. J. Shaw, “Integrated circuits based on bilayer MoS_2 transistors,” *Nano Lett.*, vol. 12, no. 9, pp. 4674–4680, Aug. 2012, doi: 10.1021/nl302015v.

[6] W. Wu, L. Wang, R. Yu, S. H. Wei, J. Hone, and Z. L. Wang, “Piezophototronic effect in single-atomic-layer MoS_2 for strain-gated flexible optoelectronics,” *Adv. Mater.*, vol. 28, no. 38, pp. 8463–8468, Aug. 2016, doi: 10.1002/adma.201602854.

[7] N. Choudhary *et al.*, “Directly deposited MoS_2 thin film electrodes for high performance supercapacitors,” *J. Mater. Chem. A*, vol. 3, no. 47, pp. 24049–24054, Oct. 2015, doi: 10.1039/c5ta08095a.

[8] D. Sarker, W. Liu, X. Xiw, A. C. Anselmo, S. Mitragotri, and K. Banerjee, "MoS_2 field-effect transistor for next-generation label-free biosensors," *ACS Nano*, vol. 8, no. 4, pp. 3992–4003, Mar. 2014, doi: 10.1021/nn5009148.
[9] W. Wu *et al.*, "Piezoelectricity of single-atomic-layer MoS_2 for energy conversion and piezotronics," *Nature*, vol. 514, p. 470, Oct. 2014, doi: 10.1038/nature13792.
[10] A. Arab and Q. Li, "Anisotropic thermoelectric behavior in armchair and zigzag mono- and fewlayer MoS_2 in thermoelectric generator applications," *Sci. Rep.*, vol. 5, Sep. 2015, Art. no. 13706, doi: 10.1038/srep13706.
[11] H. Wang *et al.*, "Large-scale 2D electronics based on single-layer MoS_2 grown by chemical vapor deposition," in *Proc. Int. Electron Devices Meeting*, San Francisco, CA, USA, 2012, pp. 4–6, doi: 10.1109/IEDM.2012.6478980.
[12] K. K. H. Smithe, S. V. Suryavanshi, M. M. Rojo, A. D. Tedjarati, and E. Pop, "Low variability in synthetic monolayer MoS_2 devices," *ACS Nano*, vol. 11, no. 8, pp. 8456–8463, Jul. 2017, doi: 10.1021/acsnano.7b04100.
[13] K. Dolui, I. Rungger, C.-D. Pemmaraju, and S. Sanvito, "Possible doping strategies for MoS_2 monolayers: An AB initio study" *Phys. Rev. B, Condens. Matter*, vol. 88, no. 7, Aug. 2013, Art. no. 075420, doi: 10.1103/PhysRevB.88.075420.
[14] T. Ohashi *et al.*, "Multi-layered MoS_2 film formed by high-temperature sputtering for enhancement-mode nMOSFETs," *Jpn. J. Appl. Phys.*, vol. 54, no. 4, Mar. 2015, Art. no. 04DN08, doi: 10.7567/JJAP.54.04DN08.
[15] T. Sakamoto *et al.*, "Mechanism for high hall-effect mobility in sputtered-MoS_2 film controlling particle energy," in *Proc. S3S Conf.*, Burlingame, CA, USA, pp. 1–2, 2018, doi: 10.1109/S3S.2018.8640168.
[16] G. Kogo *et al.*, "A thin film efficient pn-junction thermoelectric device fabricated by self-align shadow mask," *Sci. Rep.*, vol. 10, p. 1067, Jan. 2020, doi: 10.1038/s41598-020-57991-y.
[17] K. Matsuura *et al.*, "Low-carrier-density sputtered MoS_2 film by vapor-phase sulfurization," *J. Elect. Mater.*, vol. 47, no. 7, pp. 3497–3501, Mar. 2018, doi: 10.1007/s11664-018-6191-z.
[18] S. Imai *et al.*, "Important of MoS_2-compound sputtering even with sulfur-vapor anneal for chip-size fabrication," in *Proc. Int. Conf. Solid-State Devices Mater. VIRTUAL Conf.*, 2020, pp. 503–504.
[19] K. Matsuura *et al.*, "Sputter-deposited-MoS_2 n MISFETs with top-gate and Al_2O_3 passivation under low thermal budget for large area integration," *IEEE J. Electron Devices Soc.*, vol. 6, pp. 1246–1252, Nov. 2018, doi: 10.1109/JEDS.2018.2883133.
[20] S. Tongay *et al.*, "Defects activated photoluminescence in two-dimensional semiconductors: Interplay between bound, charged and free excitons," *Sci. Rep.*, vol. 3, p. 2657, Sep. 2013, doi: 10.1038/srep02657.
[21] D. Liu, Y. Guo, L. Fang, and J. Robertson, "Sulfur vacancies in monolayer MoS_2 and its electrical contacts," *Appl. Phys. Lett.*, vol. 103, no. 18, Oct. 2013, Art. no. 183113, doi: 10.1063/1.4824893.
[22] B. Akdim, R. Pachter, and S. Mou, "Theoretical analysis of the combined effects of sulfur vacancies and analyte adsorption on the electronic properties of single-layer MoS_2," *Nanotechnology*, vol. 27, no. 18, Mar. 2016, Art. no. 185701, doi: 10.1088/0957-4484/27/18/185701.
[23] S. M. Sze and K. K. Ng, *Physics of Semiconductor Devices*, 3rd ed. Hoboken, NJ, USA: Wiley, 2006, pp. 21–23.
[24] G. V. Resta *et al.*, "Polarity control in WSe_2 double-gate transistors," *Sci. Rep.*, vol. 6, Jul. 2016, Art. no. 29448, doi: 10.1038/srep29448.
[25] D. Kiriya, M. Tosun, P. Zhao, J. S. Kang, and A. Javey, "Air-stable surface charge transfer doping of MoS_2 by benzyl viologen," *J. Amer. Chem. Soc.*, vol. 136, no. 22, pp. 7853–7856, May 2014, doi: 10.1021/ja5033327.
[26] D. M. Sim *et al.*, "Controlled doping of vacancy-containing few-layer MoS_2 *via* highly stable thiol-based molecular chemisorption," *ACS Nano*, vol. 9, no. 12, pp. 12115–12123, Oct. 2015, doi: 10.1021/acsnano.5b05173.
[27] C. J. L. de la Rosa *et al.*, "Highly efficient and stable MoS_2 FETs with reversible n-doping using a dehydrated poly(vinyl-alcohol) coating," *Nanoscale*, vol. 9, no. 258, pp. 258–265, Nov. 2016, doi: 10.1039/C6NR06980K.
[28] M. Chen *et al.*, "Stable few-layer MoS_2 rectifying diodes formed by plasma-assisted doping," *App. Phys. Lett.*, vol. 103, no. 14, Oct. 2013, Art. no. 142110, doi: 10.1063/1.4824205.
[29] A. Nipane, D. Kamakar, N. Kaushik, S. Karande, and S. Lodha, "Few-layer MoS_2p-type devices enabled by selective doping using low energy phosphorus implantation," *ACS Nano*, vol. 10, no. 2, pp. 2128–2137, Jan. 2016, doi: 10.1021/acsnano.5b06529.
[30] A. Azcatl *et al.*, "Covalent nitrogen doping and compressive strain in MoS_2 by remote N_2 plasma exposure," *Nano Lett.*, vol. 16, no. 9, pp. 5437–5443, Aug. 2016, doi: 10.1021/acs.nanolett.6b01853.
[31] R. Murray, K. Haynes, X. Zhao, S. Perry, C. Hatem, and K. Jones, "The effect of low energy Ion implantation on MoS_2," *ECS J. Solid-State Sci. Technol.*, vol. 5, no. 11, pp. Q3050–Q3053, Aug. 2016, doi: 10.1149/2.0111611jss.
[32] L. Yang *et al.*, "Chloride molecular doping technique on 2D materials: WS_2 and MoS_2," *Nano. Lett.*, vol. 14, no. 11, pp. 6275–6280, Oct. 2014, doi: 10.1021/nl502603d.
[33] L. Yang *et al.*, "High-performance MoS_2 field-effect transistors enabled by chloride doping: Record low contact resistance (0.5 kΩ µm) and record high drain current (460 µA/µm)," in *Proc. Symp. VLSI Technol.*, Jun. 2014, pp. 1–2, doi: 10.1109/VLSIT.2014.6894432.
[34] B. Radisavljevic, M. B. Whitwick, and A. Kis, "Small-signal amplifier based on single-layer MoS_2," *Appl. Phys. Lett.*, vol. 101, no. 4, Jul. 2012, Art. no. 043103, doi: 10.1063/1.4738986.
[35] F. Guo, Z. Liu, M. Zhu, and Y. Zheng, "Electron-phonon scattering limited hole mobility at room temperature in a MoS_2 monolayer: First-principles calculations," *Phys. Chem. Chem. Phys.*, vol. 21, no. 41, pp. 22879–22887, Sep. 2019, doi: 10.1039/c9cp04418c.
[36] Y. Okada *et al.*, "Resistivity reduction of low-carrier-density sputtered-MoS_2 film using fluorine gas," in *Proc. 17th Int. Workshop Junction Technol. (IWJT)*, 2017, pp. 44–66, doi: 10.23919/IWJT.2017.7966510.
[37] T. Hamada, S. Yamaguchi, T. Horiguchi, K. Kakushima, K. Tsutsui, and H. Wakabayashi, "Comparative and systematic study of doping technology for 2D-sputtered MoS_2 film," in *Proc. Mater. Res. Meeting*, Yokohama, Japan, 2019, pp. 12–25.
[38] G. K. Reeves, "Specific contact resistance using a circular transmission line model," *Solid-State Electron.*, vol. 23, no. 5, pp. 487–490, May 1980, doi: 10.1016/0038-1101(80)90086-6.
[39] A. J. Willis and A. P. Botha, "Investigation of ring structures for metal-semiconductor contact resistance determination," *Thin Solid Films*, vol. 146, no. 1, pp. 15–20, Jan. 1987, doi: 10.1016/0040-6090(87)90335-X.
[40] M. Toyama *et al.*, "Ohmic contact between titanium and sputtered MoS_2 films achieved by forming-gas annealing," *Jpn. J. Appl. Phys.*, vol. 57, no. 7S2, Jun. 2018, Art. no. 07MA04, doi: 10.7567/JJAP.57.07MA04.
[41] K. S. Kim, K. H. Kim, Y. J. Ji, and G. Y. Yeom, "Layer control of 2D-MoS_2 by atomic layer etching and its device characteristics," *ECS Trans.*, vol. 86, no. 6, pp. 69–74, Jul. 2018, doi: 10.1149/08606.0069ecst.
[42] C. Tian and S. W. Chan, "Electrical conductivities $(CeO_2)_{1-x}(Y_2O_3)_x$ of thin films," *J. Amer. Ceram. Soc.*, vol. 85, no, 9, pp. 2222–2229, Dec. 2004, doi: 10.1111/j.1151-2916.2002.tb00439.x.
[43] H. Qiu *et al.*, "Hopping transport through defect-induced localized states in molybdenum disulphide," *Nat. Commun.*, vol. 4, no. 1, pp. 1–6, Dec. 2014, doi: 10.1038/ncomms3642.
[44] S. Shin, Z. Jin, D. H. Kwon, R. Bose, and Y. S. Min, "High turnover frequency of hydrogen evolution reaction on amorphous MoS_2 thin film directly grown by atomic layer deposition," *Langmuir*, vol. 31, no, 3, pp. 1196–1202, Oct. 2015, doi: 10.1021/la504162u.
[45] M. R. Laskar *et al.*, "p-type doping of MoS_2 thin films using Nb," *Appl. Phys. Lett.*, vol. 104, no. 9, Mar. 2014, Art. no. 092104, doi: 10.1063/1.4867197.
[46] J. Suh *et al.*, "Doping against the native propensity of MoS_2: Degenerate hole doping by cation substitution," *Nano Lett.*, vol. 14, no. 12, pp. 6976–6982, Nov. 2014, doi: 10.1021/nl503251h.
[47] G. Mirabelli *et al.*, "Back-gated Nb-doped MoS_2 junctionless field-effect-transistors," *AIP Adv.*, vol. 6, no. 2, Feb. 2016, Art. no. 025323, doi: 10.1063/1.4943080.
[48] T. Momose, A. Nakamura, M. Daniel, and M. Shimomura, "Phosphorous doped p-type MoS_2 polycrystalline thin films via direct sulfurization of Mo film," *AIP Adv.*, vol. 8, no. 2, Feb. 2018, Art. no. 025009, doi: 10.1063/1.5019223.
[49] K. Jo, J. Choia, and H. Kim, "Phosphorous doped p-type MoS_2 polycrystalline thin films via direct sulfurization of Mo film," *J. Mater. Chem.*, vol. 5, no. 22, pp. 5395–5401, May 2017, doi: 10.1039/c7tc01099k.

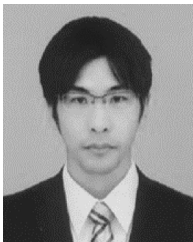

TAKUYA HAMADA received the M.E. degree in electrical engineering from the Tokyo Institute of Technology, Japan, in 2019, where he is currently pursuing the Doctoral degree.

SHIGETAKA TOMIYA received the B.S. and M.S. degrees in physics and the Ph.D. degree in electronics engineering from Keio University, Japan, in 1986, 1988, and 1999, respectively.

In 1988, he joined the Sony Corporation Research Center, Yokohama, Japan. He has engaged in the material analysis of compound semiconductors and the development of (mainly ZnSe- and GaN-based) short-wave laser diodes. He was with the University of California at Santa Barbara, Santa Barbara, CA, USA, as a Visiting Researcher from 1991 to 1992, where he engaged in novel quantum structures. Following that, he has engaged in various electronic material systems for sensors and optical devices. He is currently a Distinguished Researcher of Sony Corporation, Atsugi, Japan, and is a specially appointed Professor with the Tokyo Institute of Technology, Yokohama, Japan.

Dr. Tomiya has served as a Vice-Chair of the Committee of Manufacturing Process Innovation by Materials Informatics of JSPS, from 2016 to 2019.

TETSUYA TATSUMI received the B.S. and M.S. degrees from Waseda University in 1987 and 1989, respectively, and the Ph.D. degree from Keio University in 2000. He joined the Sony Corporation in 1989, and was engaged in the development of plasma technology for various semiconductor devices. He was a Member of the Association for Super Advanced Electronics Technology from 1997 to 2001, where he led the basic research on dry etching plasma. He is currently a Distinguished Engineer with the Sony Semiconductor Solutions Corporation and a specially appointed Professor with the Tokyo Institute of Technology. He has been awarded a Fellow of the Japanese Society of Applied Physics, since 2015.

MASAYA HAMADA received the M.E. degree in electrical engineering from the Tokyo Institute of Technology, Japan, in 2019, where he is currently pursuing the Doctoral degree.

TAIGA HORIGUCHI received the B.E. degree in electrical engineering from the Tokyo Institute of Technology, Japan, in 2020, where he is currently pursuing the master's degree.

KUNIYUKI KAKUSHIMA (Member, IEEE) received the B.S., M.S., and Ph.D. degrees in electrical engineering from the University of Tokyo, Japan, in 1999, 2001, and 2004, respectively.

He is currently an Associate Professor with the Tokyo Institute of Technology, Yokohama, Japan.

KAZUO TSUTSUI (Senior Member, IEEE) received the B.E., M.E., and Ph.D. degrees in electrical engineering from the Tokyo Institute of Technology, Japan, in 1981, 1983, and 1986, respectively.

He was with the Tokyo Institute of Technology, as a Research Associate with the Department of Physical Electronics and Department of Applied Electronics from 1986 to 1990 and as an Associate Professor with the Department of Applied Electronics from 1990 to 2010. He is a Professor with the Institute of Innovative Research, Tokyo Institute of Technology. His research interests are in the field of semiconductor electron devices, process technologies, and related characterization. He is the Fellow of Japan Society of Applied Physics, a Senior Member of the IEEE Electron Device Society, a Member of the Electrochemical Society, and a Member of the Institute of Electronics, Information, and Communication Engineers.

HITOSHI WAKABAYASHI (Senior Member, IEEE) received the M.E. and Ph.D. degrees in electrical engineering from the Tokyo Institute of Technology, Japan, in 1993 and 2003, respectively. He was with the NEC Corporation from 1993 to 2006, the Massachusetts Institute of Technology from 2000 to 2001, and Sony Corporation from 2006 to 2012. He has been with the Tokyo Institute of Technology, since 2013. He was a recipient of the Young Scientist Presentation Award 2000 of JSAP. He has served as the Chair of VLSI Technology and Circuits Committee, EDS, and the General Chair for Symposium on VLSI Technology 2013, EDTM 2018, and IWJT 2017/2019/2021.